(e,p) and (e,α) reactions in ^{90}Zr and ^{92}Zr

W. R. Dodge and Evans Hayward
National Bureau of Standards, Gaithersburg, Maryland 20899

M. N. Martins and E. Wolynec
Laboratorio do Acelerador Linear, Instituto de Fisica de Universidade de Sao Paulo, Sao Paulo, SP, Brazil

(Received 23 May 1985)

The yields of protons and α particles from 2 mg/cm^2 targets of ^{90}Zr and ^{92}Zr have been measured in the incident electron energy range 20—100 MeV; the ^{90}Zr(e,p) and ^{90}Zr(e,α) data were extended to 130 MeV. Photodisintegration plus electrodisintegration yields were also measured for electron energies above 50 MeV. The photodisintegration cross sections, derived from these data, rise continuously from 25 MeV onward for all four reactions. One satisfactory explanation of this phenomenon is that we are observing multiparticle emission following virtual photon absorption.

I. INTRODUCTION

Some time ago Tamae *et al.*[1] reported on a measurement of the ^{90}Zr(e,α) cross section and the photonuclear cross section derived from it. The latter contained a peak resulting from the $E1$ giant resonance as well as an increasing cross section above 30 MeV. At the highest excitation energy measured by Tamae *et al.*,[1] 60 MeV, the cross section exceeded the giant dipole cross section. This curious feature led us to embark on a measurement of the (e,p) and (e,α) cross sections of ^{90}Zr and ^{92}Zr in the hope of reaching some understanding of this interesting phenomenon.

II. EXPERIMENT

The (e,p) and (e,α) cross sections for ^{90}Zr and ^{92}Zr have been measured in the incident electron energy range 20—100 MeV. The ^{90}Zr measurements were extended to 130 MeV. The experimental apparatus and the National Bureau of Standards (NBS) linear electron accelerator have been described previously.[2–4] Target thicknesses, isotopic purities, and the separation energies for the decay channels of interest are presented in Table I. For electron energies between 50 and 100 MeV photodisintegration plus electrodisintegration yields were measured by interposing a 136 mg/cm^2 Ta radiator 7.6 cm upstream of the Zr targets. The effects of multiple scattering and electron energy loss in the 136 mg/cm^2 radiator used were checked with a 217 mg/cm^2 radiator at 60 and 100 MeV in a previous experiment.[5] At these energies when the electrodisintegration yields were subtracted from the photodisintegration plus electrodisintegration yields for both radiators, the (counts/Coulomb) (mg/cm^2) of radiator were the same within counting statistics.

Five silicon surface barrier charged particle detectors were mounted in the spectrometer focal plane. Three of these detectors were 10×40 mm rectangular detectors and two were 22 mm circular detectors. All detectors could be totally depleted. The absolute efficiency of the ith counter is defined to be

$$(\text{Efficiency})_i = \frac{\int C(p)_i d\Omega\, dp}{4\pi S_0}\ , \tag{1}$$

TABLE I. Separation energies and target properties.

Reaction	Separation energy ^{90}Zr (MeV)	Separation energy ^{92}Zr (MeV)
(γ,p)	8.36	9.40
(γ,n)	11.98	8.64
(γ,2p)	15.43	17.11
(γ,np)	19.83	17.34
(γ,2n)	21.29	15.84
(γ,n2p)	26.55	24.91
(γ,2np)	29.21	24.20
(γ,n3p)	35.96	35.79
(γ,3np)	37.82	35.67
(γ,n4p)	48.16	44.99
(γ,4np)	50.50	45.05
(γ,n5p)	55.40	57.01
(γ,5np)	62.72	56.87
(γ,α)	6.68	2.97
(γ,2α)	13.02	10.87
(γ,αp)	16.32	13.58
(γ,αn)	18.16	14.09
(γ,3α)	19.01	17.97
(γ,2αp)	22.93	21.58
(γ,2αn)	24.01	21.39
(γ,4α)	25.04	24.94
(γ,αnp)	26.80	23.50
(γ,3αp)	29.41	29.33
(γ,3αn)	29.51	27.87
(γ,2αpn)	33.09	31.16
(γ,4αn)	35.24	34.39
(γ,4αp)	36.01	36.91
Enrichment (%)	97.62	95.13
Thickness (mg/cm^2)	2.02	2.00

where $C(p)_i$ stands for the number of counts recorded by a focal plane counter when a calibrated alpha source of strength S_0 is located in the target position of the spectrometer. Relative values of the efficiencies obtained from alpha source measurements agreed within counting statistics with a series of measurements made with each counter measuring protons and alphas of the same energy from a smooth portion of a (e,p) or (e,α) energy spectrum. The centroid of the distribution $C(p)_i$ provided the spectrometer momentum calibration for the ith counter. ^{241}Am and ^{238}U calibrated alpha sources provided by the NBS radioactivity section were used for these measurements. The dependence of the counter efficiency on beam spot size was determined by direct comparison of the counting rate with a 2 mm beam spot and with a 22 mm beam spot. The counting rates under these two extreme conditions differed by only 4.5%. Since the beam size did not exceed 10 mm even at the lowest electron energy, we assumed our counting efficiency was independent of electron energy.

For each target complete electrodisintegration energy spectra, $d^2\sigma/d\Omega\, dT$, were taken at 90° for incident electron energies, E_0, of 20, 22, 24, 30, 40, 50, 60, 80, and 100 MeV. Complete photodisintegration plus electrodisintegration energy spectra were taken at 50, 60, 80, and 100 MeV. At other incident electron energies, E_0, between 20 and 100 MeV, the proton and α-particle cross sections were sampled in 2 MeV steps at a single magnetic field setting of the spectrometer roughly corresponding to the peak of the α-particle cross section. These cross sections were also measured in 5 MeV steps for ^{90}Zr between 100 and 130 MeV. These "bite" cross section measurements were converted into complete cross sections by using ratios, $R_\alpha(E_0)$ and $R_p(E_0)$, obtained from the complete cross section measurements. The ratios $R_\alpha(E_0)$ and $R_p(E_0)$ were defined to be

$$R_i(E_0)=\frac{\int_{T_{\text{thres}}}^{T_{\max}}(d^2\sigma/d\Omega\, dT)_i dT}{\int_{T_{\text{bite}}}(d^2\sigma/d\Omega\, dT)_i dT}\ . \tag{2}$$

The contribution to the (e,α) and (e,p) yields from the energy region, which lies above the maximum energy which the spectrometer magnet can bend ($\approx$25 MeV), was estimated by using the α-particle data of Flowers *et al.*[6] for ^{92}Mo and ^{94}Mo, and the proton data of Schumacher *et al.*[7] for Cu, and Tonapetyan *et al.*[8] for ^{93}Nb. In the energy region above 20 MeV both the proton and α-particle energy distributions are approximately given by

$$\frac{d^2\sigma}{d\Omega\, dT_i}=\left[\frac{d^2\sigma}{d\Omega\, dT_i}\right]_0 e^{-\lambda T_i}\ , \tag{3}$$

with

$$\lambda_\alpha=(0.16\pm0.02)/\text{MeV}$$

and

$$\lambda_p=(0.021\pm0.003)/\text{MeV}\ .$$

These values of λ are nearly constant for a wide range of mass numbers A (λ_p=0.021/MeV for ^{93}Nb at a bremsstrahlung end-point energy of 340 MeV and 0.023/MeV for Cu at end-point energies of 150 and 340 MeV). The values $R_p(E_0)$ and $R_\alpha(E_0)$ are given in Tables II and III. Where a second set of values for $R_p(E_0)$ is given, it includes an estimate of the proton yield above 25 MeV. These larger values were used to evaluate the (e,p) cross sections. The high-energy tail for the α particles made a negligible contribution. The larger value of $R_\alpha(E_0)$ at each E_0 contains the α yield below 5.6 MeV displayed in Fig. 2. The cross sections were evaluated excluding the yield below 5.6 MeV since we believe it is produced by a contaminant. Since $R_\alpha(E_0)$ and $R_p(E_0)$ were slowly varying functions of E_0 except within a few MeV of the threshold energies, these ratios between measured values were obtained by a linear interpolation and only the error estimate of the bite area and the ratios $R_\alpha(E_0)$ and $R_p(E_0)$ were included in the error estimate of the total cross section.

The linac beam currents were measured with an NBS beam dump during electrodisintegration measurements

TABLE II. The ratio, R_p, defined in Eq. (2) as a function of the incident electron energy, E_0. Where a second set of ratios is given, it includes an estimate of the proton yield above 25 MeV (see the text for details).

E_0	^{90}Zr(e,p)	^{90}Zr(e + γ,p)	^{92}Zr(e,p)	^{92}Ze(e + γ,p)
20	60.8 ±1.9		79.9±4.3	
22	20.24±0.20		13.8±0.2	
24	18.9 ±0.2		10.6±0.2	
30	17.4 ±0.2		10.9±0.1	
	17.6 ±0.2		11.0±0.1	
40	17.0 ±0.2		11.3±0.1	
	17.9 ±0.2		12.3±0.1	
50	15.9 ±0.1	16.0±0.1	10.7±0.1	10.9±0.1
	17.0 ±0.2	17.1±0.2	11.9±0.2	12.1±0.2
60	16.7 ±0.1	16.4±0.1	11.7±0.1	11.8±0.1
	17.7 ±0.1	19.9±0.1	12.5±0.2	12.5±0.2
80	16.1 ±0.1	16.5±0.1	11.9±0.1	11.9±0.1
	17.3 ±0.2	17.9±0.1	13.3±0.3	13.5±0.1
100	15.8 ±0.1	15.9±0.1	11.7±0.1	11.6±0.1
	18.1 ±0.1	18.4±0.2	15.1±0.2	14.5±0.2

TABLE III. The ratio, R_α, defined in Eq. (2) as a function of the incident electron energy, E_0. The second set of ratios given at each E_0 do not include the alpha yield below 5.6 MeV (see the text for details).

E_0	^{90}Zr(e,α)	^{90}Zr(e + γ,α)	^{92}Zr(e,α)	^{92}Ze(e + γ,α)
20	4.65±0.31		2.94±0.11	
	4.19±0.20		2.87±0.11	
22	4.24±0.20		2.91±0.10	
	3.79±0.17		2.81±0.09	
24	3.73±0.13		2.92±0.09	
	3.43±0.12		2.81±0.09	
30	3.79±0.15		3.21±0.07	
	3.50±0.14		3.11±0.07	
40	4.12±0.12		3.30±0.08	
	3.76±0.11		3.15±0.08	
50	4.23±0.10	4.04±0.06	3.63±0.08	3.61±0.05
	3.86±0.10	3.73±0.06	3.61±0.08	3.46±0.05
60	4.50±0.05	4.42±0.05	4.01±0.07	4.01±0.05
	4.06±0.04	4.02±0.04	3.80±0.06	3.76±0.04
80	4.84±0.07	4.81±0.06	4.43±0.07	4.43±0.05
	4.35±0.05	4.43±0.05	4.06±0.06	4.16±0.05
100	4.81±0.06	4.87±0.04	4.62±0.06	4.62±0.05
	4.48±0.07	4.54±0.04	4.39±0.04	4.37±0.04

and with a ferrite beam current monitor calibrated relative to the beam dump during radiator-in measurements. Alpha particles and protons were separated by varying the bias of the silicon transmission detectors so that protons were not stopped in the depletion layer while alphas were always stopped except at the highest fields where the range of the alphas exceeded the thickness of the detectors.

III. RESULTS

The proton energy spectra, $(d^2\sigma/d\Omega\, dT_p)$, from ^{90}Zr and ^{92}Zr bombarded with 20 MeV electrons are shown in Fig. 1. All of the structure seen in the ^{90}Zr energy spectrum has been reported previously.[9–14] The strong state which occurs at a center-of-mass proton energy of 7.94 MeV, corresponding to an excitation energy of 16.28 MeV, is a 1^- analog state which has been widely studied. The peak at 6.40 MeV results from the decay of the 16.28 MeV state to the 1.51 MeV, $\frac{3}{2}^-$ second excited state in ^{89}Y. The peak at 6.00 MeV is the ground state decay of a 1^- analog state with an excitation energy of 14.43 MeV. The energy difference between the small peak at 4.9 MeV and the 6.40 MeV peak suggests that the 4.9 MeV peak is due to the decay of the 14.43 MeV 1^- state to the 1.51 MeV, $\frac{3}{2}^-$ second excited state in ^{89}Y.

The prominent peak near 4 MeV has been reported extensively.[9–12,14,15] This peak is thought to be a pseudoresonance produced by the opening of the neutron channel at an effective threshold of 12.568 MeV.[12] Since the ground state of ^{89}Zr is $\frac{9}{2}^+$, ground-state neutron transitions are strongly inhibited by the angular momentum barrier, and the neutron channel remains effectively closed until the first excited $\frac{1}{2}^-$ state at 0.588 MeV is energetically feasible. Since the total photon-absorption cross section should be smooth, the behavior of the (γ,p) cross section implies a very sharp rise in the (γ,n) cross section near threshold.

Although the ^{92}Zr(γ,n) reaction has been well studied,[16] the ^{92}Zr(γ,p) reaction has not been reported in the literature. The strong peak seen at 7.38 MeV in Fig. 1(b) probably results from ground-state transitions from a 1^- ana-

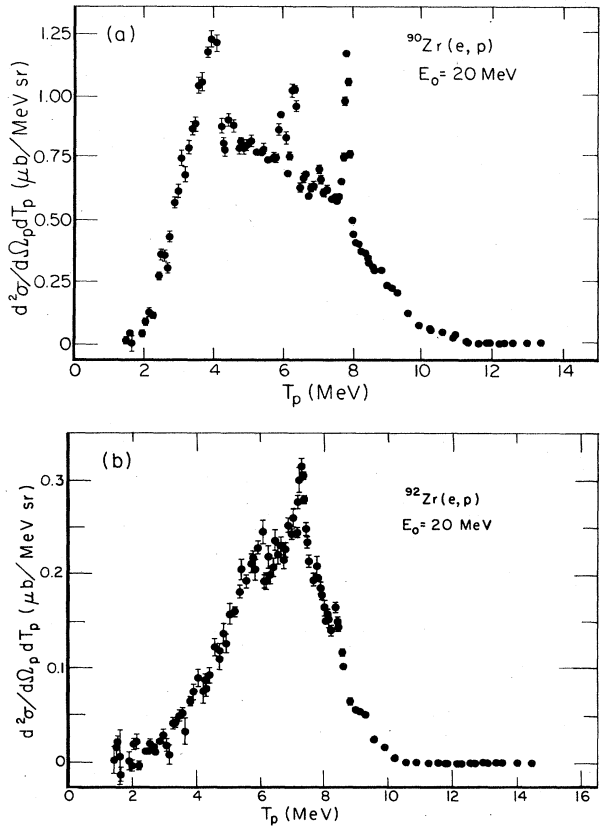

FIG. 1. The proton spectra produced at 90° when 20 MeV electrons are incident on targets of ^{90}Zr and ^{92}Zr.

log state at an excitation energy of 16.8 MeV. The smaller peaks seen at 7.03 and 5.90 MeV are probably the decays of the 16.8 MeV state to the $\frac{3}{2}^-$ excited states at 0.556 and 1.474 MeV in ^{91}Y. The pseudoresonance found in the ^{90}Zr spectrum is, of course, not seen here, because the neutron separation energy is less than the proton separation energy.

The α spectra for ^{90}Zr and ^{92}Zr, $(d^2\sigma/d\Omega\, dT_\alpha)$, observed at 90° using 60 MeV incident electrons are shown in Figs. 2(a) and (b). They have a peak characteristic of evaporation spectra for α-particle energies near the Coulomb barrier height. The high-energy tails of the α spectra are usually associated with preequilibrium processes.[6]

Both of these spectra display a group of α particles near 3 MeV. It is hard to understand how α particles of such low energy could survive the Zr Coulomb barrier. We believe that they are produced in the ^{12}C(e,3α) reaction because (1) there is a dark spot on the targets the size and shape of the beam and (2) after a 30-minute exposure to 30 MeV electrons there was a component in the decay curve of the annihilation radiation having a half-life consistent with that of ^{11}C. For this reason the low-energy yield in the α spectra has been excluded in the evaluation of the cross sections.

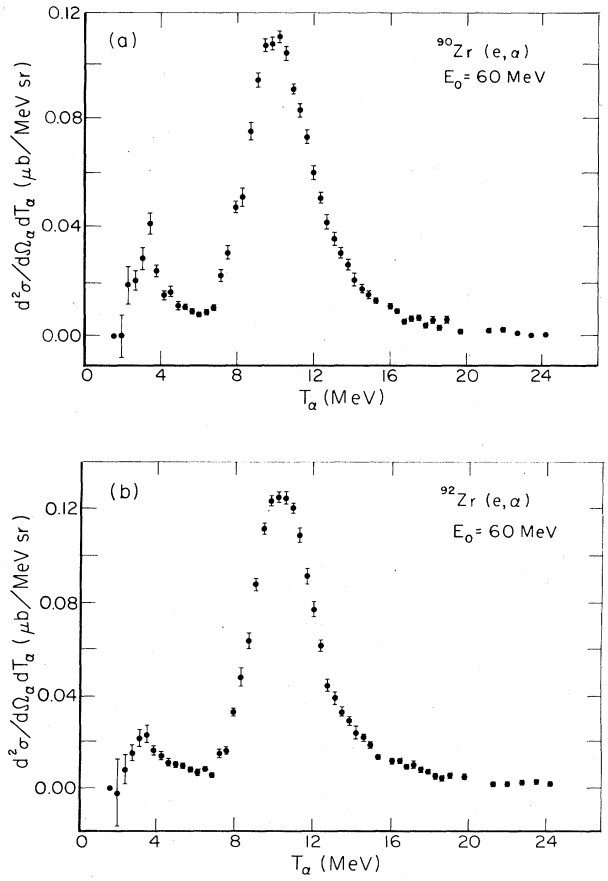

FIG. 2. The α-particle spectra produced at 90° when 60 MeV electrons are incident on targets of ^{90}Zr and ^{92}Zr.

IV. DATA ANALYSIS

The data were treated in much the same way as described in Ref. 4. The measured spectra, $d^2\sigma/d\Omega\, dT$, were integrated over particle energy to obtain $d\sigma/d\Omega$ (90°), and the latter was multiplied by 4π to yield the total cross section, $\sigma_{e,x}(E_0)$. The photodisintegration plus electrodisintegration yields, $Y_{e,x}(E_0)$, were obtained by multiplying by the same factors. These two measured quantities, $\sigma_{e,x}(E_0)$ and $Y_{e,x}(E_0)$, are plotted as a function of total incident electron energy, E_0, in Figs. 3–6 for the four reactions studied here.

The relationship between the photodisintegration cross section, $\sigma_{\gamma,x}(E_0)$, and the measured electrodisintegration cross section is

$$\sigma_{e,x}(E_0)=\int_0^{E_0-m}\sum_{\lambda L}\sigma_{\gamma,x}^{\lambda L}(\omega)N^{\lambda L}(E_0,\omega,Z)\frac{d\omega}{\omega}\ , \quad (4)$$

where $N^{\lambda L}(E_0,\omega,Z)$ is the virtual photon intensity spectrum of multipolarity λL. The yield with the radiator in is

$$Y_{e,x}(E_0)=\sigma_{e,x}(E_0-2\Delta E_0)+n_r\int_0^{E_0-m}\sum_{\lambda L}\sigma_{\gamma,x}^{\lambda L}(\omega)K(E_0-\Delta E_0,\omega)\frac{d\omega}{\omega}\ . \quad (5)$$

Here n_r is the number of nuclei/cm^2 in the tantalum radiator and ΔE_0 is the electron energy loss in half the radiator thickness. For the bremsstrahlung cross section, $K(E_0,\omega)$, we have used the Davies-Bethe-Maximon cross section as given in Ref. 17.

The cross sections, $\sigma_{e,x}(E_0)$, and yields, $Y_{e,x}(E_0)$, of Figs. 3–6 have been simultaneously fitted using the $E1$

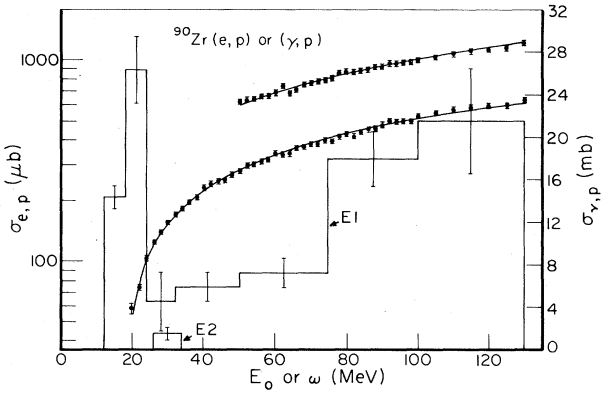

FIG. 3. The measured $\sigma_{e,p}(E_0)$ for ^{90}Zr as a function of total incident electron energy E_0 (lower points). The upper points represent the yield $Y_{e,p}(E_0)$ obtained when a 0.136 g/cm^2 tantalum foil was placed in the electron beam ahead of the target. The smooth curves are the best fits to the data and were obtained by combining the histograms representing the $E1$ and $E2$ (γ,p) cross sections (right-hand scale) in Eqs. (1) and (2) with the $E1$ and $E2$ DWBA virtual photon spectra and by making use of the Davies, Bethe, and Maximom (DBM) bremsstrahlung cross section. The size effect correction described in the text has been applied to the virtual photon spectra.

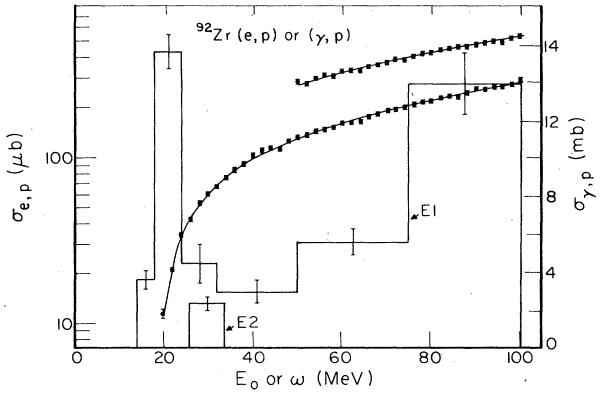

FIG. 4. The $\sigma_{e,p}(E_0)$ for ^{92}Zr. See caption of Fig. 3.

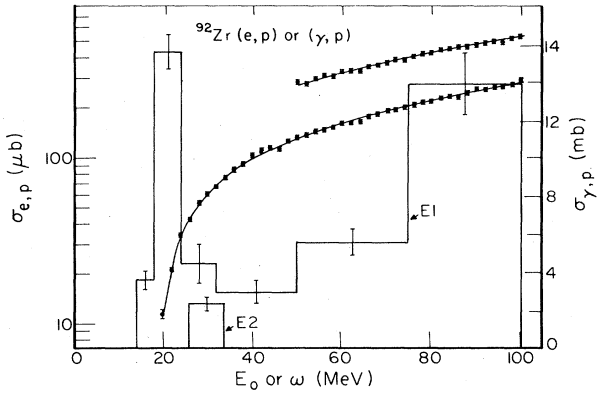

FIG. 6. The $\sigma_{e,\alpha}(E_0)$ for ^{92}Zr. See caption of Fig. 3.

and $E2$ virtual photon spectra calculated from the distorted-wave Born approximation (DWBA) code of Soto Vargas *et al.*[18] This code assumes a point nucleus and hence neglects the momentum dependence of the nuclear form factors and the interference between the nuclear form factors and the Coulomb distortion effects. We have introduced a simple expression to correct for the momentum dependence of the form factors (i.e., reduced matrix elements) which reproduces the measured rms nuclear charge radius R. This correction consists in multiplying $N^{\lambda L}(E_0,\omega,Z)$ inside the integrals of Eq. (4) and (5) by

$$F^L(qR)=\left[\left[\frac{\omega}{q}\right]^L\frac{j_L(qR)}{j_L(\omega R)}\right]^2_{q=q_{\rm rms}}. \tag{6}$$

The rms values of q were obtained in plane-wave Born approximation (PWBA) as described in Ref. 2. Because of the strong forward peaking of the $E1$ (e,e′x) cross section from which the (e,x) cross section and virtual photon spectra are derived, the model dependence of the nuclear form factor correction is very small for $E1$ transitions as long as the form factors reproduce the measured ground-state charge and transition radii.

The fits to the electrodisintegration and photodisintegration plus electrodisintegration cross sections are shown in Figs. 3—6, the photodisintegration cross sections being represented by very coarse histograms. The $E2$ strength is represented by a single bin at the energy of the isovector $E2$ resonance. Durgapal and Onley[19] have written a second order Born approximation (SOBA) computer code which is valid for Zr. This code takes into account a certain class of nuclear form factors as well as the interference between the form factors and the Coulomb distortion. The results of using the SOBA virtual photon spectra to analyze our data are the second entries in Table IV. The χ^2 test for goodness of fit are worse using the SOBA spectra without $E2$ isovector strength, but with $E2$ isovector strength both SOBA and DWBA with a multiplicative form-factor correction give roughly equally good fits.

The most remarkable feature of the derived ^{90}Zr(γ,p) and (γ,α) cross sections is that they are still rising at the highest excitation energies we sampled, 130 MeV. The same remarks apply to the ^{92}Zr(γ,p) and (γ,α) cross sections up to 100 MeV. Thus we confirm the principle result of Tamae *et al.*[1] for the ^{90}Zr(γ,α) cross section and, in addition, show that the "apparent cross section rise" is also seen in the ^{90}Zr(γ,p), ^{92}Zr(γ,p), and ^{92}Zr(γ,α) decay channels. We shall argue below that we believe that the apparent cross section rise is not real but due to our inability to measure more than one particle in the final state. Our ^{90}Zr(e,α) excitation function rises about 20% faster than that of Tamae *et al.*[1] in the excitation energy interval of 20 to 60 MeV and the average value of ours in this energy range is about 27% smaller than theirs.

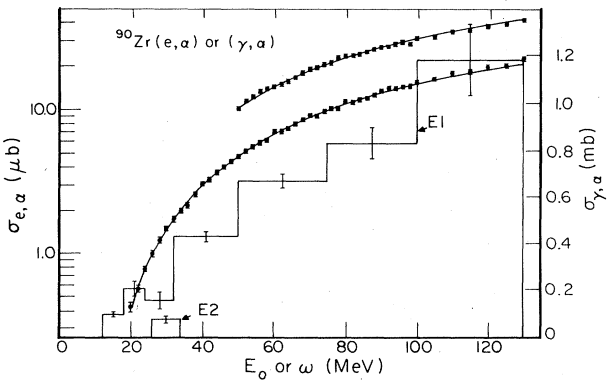

FIG. 5. The $\sigma_{e,\alpha}(E_0)$ for ^{90}Zr. See caption of Fig. 3.

V. DISCUSSION

This rather strange behavior raises the question whether (1) it is an artifact of the virtual photon spectrum used in the analysis[6] or (2) it results from multiparticle emission following virtual photon absorption. We have already shown[5] that the electric dipole virtual photon spectrum, including Coulomb distortions and nuclear size corrections, quite adequately describes the electroexcitation of a discrete level. We cannot be quite so confident concerning electrodisintegration in the quasideuteron region.

Chang *et al.*[20] and Tiator and Wright[21,22] have pointed out that the virtual photon spectra for light systems are

TABLE IV. Integrated cross sections. There are two entries for each reaction. The first is evaluated using the DWBA virtual photon spectrum with the form factor correction and the second using the SOBA spectrum.

Reaction	Reduced χ^2	$E1$ fit $\int^{30}\sigma^{E1}d\omega$ (MeV mb)	$\int_{30}^{100}\sigma^{E1}d\omega$ (MeV mb)	$\int_{30}^{130}\sigma^{E1}d\omega$ (MeV mb)
^{90}Zr(γ,α)	1.63	3.5±0.3	53.6±2.0	95.5±5.3
	2.94	3.7±0.3	55.6±2.0	93.5±5.4
^{90}Zr(γ,p)	0.74	281±25	813±77	1730±170
	1.26	305±26	785±79	1570±173
^{92}Zr(γ,α)	1.10	3.5±0.4	47.2±2.2	
	2.24	2.3±0.3	50.2±2.3	
^{92}Zr(γ,p)	1.35	149±8	664±45	
	2.33	156±8	661±64	

Reaction	Reduced χ^2	$E1$ + isovector $E2$ fit $\int^{30}\sigma^{E1}d\omega$ (MeV mb)	$\int_{30}^{100}\sigma^{E1}d\omega$ (MeV mb)	$\int_{30}^{130}\sigma^{E1}d\omega$ (MeV mb)	$\int\sigma^{E2}d\omega$ (MeV mb)
^{90}Zr(γ,α)	0.81	2.4±0.3	48.9±2.0	84.3±5.2	0.53±0.12
	2.11	2.9±0.2	52.1±2.0	91.3±5.4	6.9±0.4
^{90}Zr(γ,p)	0.65	271±20	744±147	1389±168	11.9±4.6
	0.91	280±15	695±156	1470±171	76±15
^{92}Zr(γ,α)	0.85	3.3±0.4	42.6±2.3		0.69±0.14
	1.27	3.7±0.3	47.8±2.3		1.90±0.24
^{92}Zr(γ,p)	0.60	141±9	545±46		18.7±2.8
	1.27	138±15	569±88		50.5±5.5

substantially modified by recoil effects. To test these ideas we have assumed that for excitation energies greater than ~40 MeV the dominant absorption takes place via the quasideuteron mechanism in which the $(A-2)$ system is simply a spectator and that the observed protons and α particles are generated in the final state interactions of the neutron-proton pair produced by the initial photon absorption. We have generated a virtual photon spectrum that includes exact three-body kinematics, two nucleons, and a scattered electron. Since our range of excitation energies extends beyond the region where the neglect of the Coulomb, transverse-Coulomb interference, and transverse-transverse terms of the coincidence (e,e'x) cross section is justified, we include all of the terms in a numerical calculation of the virtual photon spectrum for $A=2$. Including these terms forced us to abandon the forward peaking approximation of Tiator and Wright[21] and to work either in the long-wavelength limit (LWL) or to include model-dependent form factors in our calculation.[23] We assumed the virtual photon spectrum to be

$$N_{\rm QD}^{E1}(E_0,\omega,A,A)=\{[1-(e^{-L/\omega})]N_{\rm PWBA}^{E1}(E_0,\omega)R_{\rm FF}(E_0,\omega,Z_{\rm Zr},A_{\rm Zr}) +(e^{-L/\omega})N_{\rm QD}^{E1}(E_0,\omega,A_D)R_{\rm FF}(E_0,\omega,Z_D,A_D)\}R_C(E_0,\omega,Z)\ , \quad (7)$$

where $L\approx 80$ MeV is the Levinger quenching factor,[24] and the functions $R_{\rm FF}(E_0,\omega,Z,A)$ and $R_C(E_0,\omega,Z)$ are corrections for form factor and Coulomb distortion effects and are described more fully in Ref. 23. In the analysis of our experiment we integrate over all energies and angles of the emitted protons or α particles at each E_0. Because of the recoil of the correlated nucleon pair, decay protons of the same kinetic energy, $T_{\rm p}$, can be produced by the absorption of a range of virtual photon energies and an even wider range of virtual photon momentum transfer. The $N_{\rm QD}^{E1}(E_0,\omega)$ we require is given by

$$N_{\rm QD}^{E1}(E_0,\omega)=\int d\Omega_{\rm p}dT_{\rm p}d\Omega_{\rm e,e'} \times\frac{d^3\sigma_{\rm e,p}[E_0,T_{\rm p}(\theta_{\rm e,e'},\phi_{\rm e,e'})]}{d\Omega_{\rm p}dT_{\rm p}d\Omega_{\rm e,e'}}\ , \quad (8)$$

where the integration over the (e,e'p) coincidence cross section[23] is carried out subject to the constraint that only

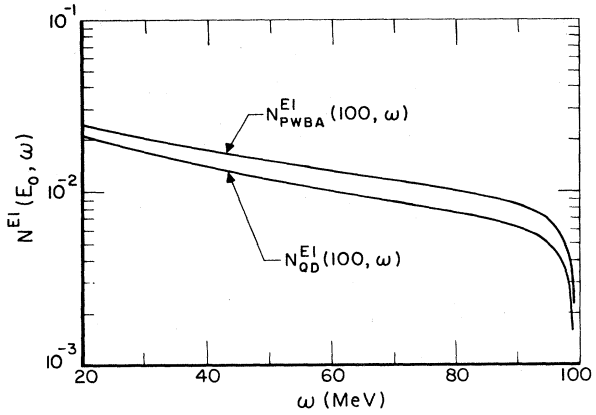

FIG. 7. The quasideuteron virtual photon spectrum $N^{E1}_{QD}(100,\omega)$ defined in Eq. (8) and the infinite mass, no recoil, spectrum $N^{E1}(100,\omega)$.

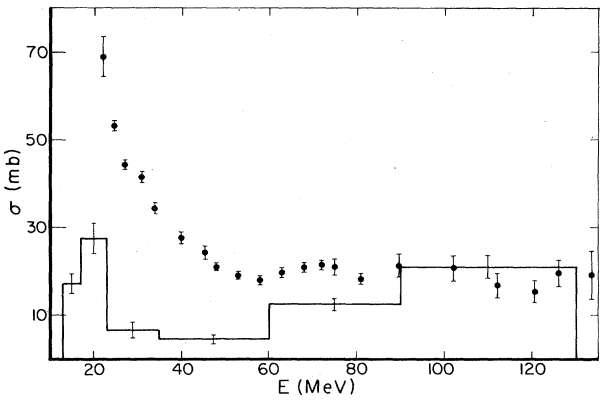

FIG. 8. A comparison of the measured ^{90}Zr proton yield cross section, $\sum_i i\sigma(\gamma,ip)$, a histogram fit similar to that of Fig. 3, with the neutron yield cross section, $\sum_i i\sigma(\gamma,in)$, reconstructed from the data of Ref. 27.

those values of $\theta_{e,e'}$, $\phi_{e,e'}$, and θ_p which produce the same ω are included in the integration. Experimental values[25,26] for the deuteron photodisintegration angular distribution coefficients, $a_0(\omega)$ and $a_2(\omega)$, were used in the evaluation of Eq. (8). After the integration of Eq. (8) over $d\Omega_{ee'}$ the result was divided by

$$a_0(\omega_\gamma)P_0(\cos\theta_{ep})+a_2(\omega_\gamma)P_2(\cos\theta_{ep})$$

and other electron kinematic variables to obtain the quasideuteron virtual photon spectrum. Without the $(\theta_{ee'},\varphi_{ee'})$ dependence introduced by recoil effects, the transverse-Coulomb and transverse-transverse terms of the coincidence cross section would not contribute to $N^{E1}_{QD}(E_0,\omega)$. $N^{E1}_{QD}(E_0,\omega)$ is shown in Fig. 7 along with the plane wave virtual photon spectrum. This alteration in the virtual photon spectrum is not adequate to eliminate the high energy rise in $\sigma(\gamma,p)$ and $\sigma(\gamma,\alpha)$ if only $E1$ virtual photon absorption is important. The high energy rise in the (e,p) cross section can be eliminated by multiplying the Levinger quenching factor, $e^{-L/\omega}$, in Eq. (7) by an arbitrary function of ω; however, the same modification of the virtual photon spectrum of Eq. (7) will not eliminate the high energy rise in the (e,α) cross section but only reduce its magnitude slightly. Moreover, such modifications to the virtual photon spectra will not allow satisfactory simultaneous fits to be obtained to both our electroexcitation data and our bremsstrahlung data, measured between 50 and 100 MeV.

Thus we are left with the alternative that the cross section rise is produced by multiparticle emission following virtual photon absorption by the quasideuteron. The quantities we have called (e,p) and (e,α) cross sections[2–4] are really photoproton and photoalpha yield cross sections and should be written as

$$\sigma_p=\sum_i i\sigma(\gamma,ip) \quad \text{and} \quad \sigma_\alpha=\sum_i i\sigma(\gamma,i\alpha)\,. \tag{9}$$

In Fig. 8 we compare our ^{90}Zr photoproton yield cross section, the histogram of Fig. 3, with the photoneutron yield cross section,

$$\sigma_n=\sum_i i\sigma(\gamma,in)\,, \tag{10}$$

reconstructed from the results of Ref. 27. The two curves come together for energies above 90 MeV suggesting that the multiplicities in the two channels are the same. In the range of 40—90 MeV some protons have low enough energies so that they cannot escape the Coulomb barrier and there neutron emission is more important. As Table I shows, the separation energies for multiple proton and alpha emission are not so high as to preclude the possibility of this explanation, especially if nucleon emission occurs predominantly in the preequilibrium stage.

The (γ,p) cross section for ^{90}Zr integrated to 30 MeV of 271±20 MeV mb is consistent with the value of 235±20 MeV mb obtained by Brajnik *et al.*,[14] especially since their cross section does not contain all transitions and ours includes some (γ,2p) reactions. The ^{92}Zr(γ,p) cross section integrated to 30 MeV is depressed with respect to that of ^{90}Zr because more dipole strength goes into neutron emission as it does for any target with excess neutrons.

In our previous experiments[2,4] the problem of multiple particle emission was certainly not so conspicuous, and except for the nucleus, ^{64}Zn, we obtained (γ,p) and (γ,α) cross sections which were flat at energies above the giant resonance. Here the yields seem to be dominated by multiparticle emission. It would be interesting to see if a precompound model calculation, analogous to the one reported by Blann *et al.*,[28] would reproduce these results.

On the experimental side it is possible and useful to study induced radioactivities, because characteristic gamma rays and half-lives serve to identify specific channels. For example, after a 130 MeV irradiation the gamma-ray spectrum from the ^{90}Zr target was examined, and the relative intensities of the gamma rays from ^{88}Y (1836 keV) and ^{88}Zr (393 keV) were determined. This comparison led to the conclusion that the ^{90}Zr (γ,2n) and (γ,pn) cross sections are comparable, lending support to our ideas

about the multiplicities. In the future it would be interesting to study the ^{90}Zr(e,3p) reaction through the induced radioactivity.

ACKNOWLEDGMENTS

The authors wish to acknowledge the joint support of Conselho Nacional de Desenvolvimento Cientifico e Tecnologico and the National Science Foundation which has made this collaboration possible. They also wish to thank T. Tamae and P. Carlos for sending their data and F. Schima for his help with the radioactivity measurements. One of the authors, W.R.D., wishes to acknowledge the hospitality of the Lewes Physics Center where part of this paper was written.

[1]T. Tamae, T. Urano, M. Hirooka, and M. Sugawara, Phys. Rev. C **21**, 1758 (1980).
[2]D. M. Skopik and W. R. Dodge, Phys. Rev. C **6**, 43 (1972).
[3]E. Wolynec, W. R. Dodge, R. G. Leicht, and E. Hayward, Phys. Rev. C **22**, 1012 (1980).
[4]W. R. Dodge, R. G. Leicht, E. Hayward, and E. Wolynec, Phys. Rev. C **24**, 1952 (1981).
[5]W. R. Dodge, E. Hayward, and E. Wolynec, Phys. Rev. C **28**, 150 (1983).
[6]A. G. Flowers, P. J. Thorley, I. Anthony, D. Branford, J. C. McGeorge, M. R. Sene, A. C. Shotter, C. H. Zimmerman, and R. O. Owens, Nucl. Phys. **A429**, 61 (1984).
[7]R. A. Schumacher, G. S. Adams, D. R. Ingham, J. L. Mathews, W. W. Sapp, R. S. Turley, R. O. Owens, and B. L. Roberts, Phys. Rev. C **25**, 2269 (1982).
[8]S. G. Tonapetyan, N. V. Goncharov, and V. M. Khvorostyan, Yad. Fiz. **22**, 433 (1975) [Sov. J. Nucl. Phys. **22**, 226 (1976)].
[9]E. Obst, F. Rauch, and E. Rossle, Phys. Lett. **21**, 50 (1966).
[10]E. Obst, F. Rauch, and H. G. Wahsweiler, Nucl. Phys. **A103**, 17 (1967).
[11]W. M. Mason, G. Kernel, J. L. Black, and N. W. Tanner, Nucl. Phys. **A135**, 193 (1969).
[12]M. Hasinoff, G. A. Fisher, and S. S. Hanna, Nucl. Phys. **A216**, 221 (1973).
[13]K. Shoda, M. Sugawara, T. Saito, and H. Miyase, Nucl. Phys. **A221**, 125 (1974).
[14]D. Brajnik, D. Jamnik, G. Kernel, M. Korun, U. Miklavzic, B. Pucelj, and A. Stanovnik, Phys. Rev. C **13**, 1852 (1976).
[15]H. J. Askin, R. S. Hicks, K. J. F. Allen, R. J. Petty, and M. N. Thompson, Nucl. Phys. **A204**, 209 (1973).
[16]B. L. Berman, J. T. Caldwell, R. R. Harvey, M. A. Kelly, R. L. Bramblett, and S. C. Fultz, Phys. Rev. **162**, 1098 (1967).
[17]J. L. Mathews and R. O. Owens, Nucl. Instrum. Methods **111**, 157 (1973).
[18]C. W. Soto Vargas, D. S. Onley, and L. E. Wright, Nucl. Phys. **A288**, 45 (1977).
[19]P. Durgapal and D. S. Onley, Phys. Rev. C **27**, 523 (1983).
[20]C. C. Chang, W. R. Dodge, and J. J. Murphy II, Phys. Rev. C **9**, 1300 (1974).
[21]L. Tiator and L. E. Wright, Nucl. Phys. **A379**, 407 (1982).
[22]L. E. Wright and L. Tiator, Phys. Rev. C **26**, 2349 (1982).
[23]W. R. Dodge, Nucl. Instrum. Methods (Phys. Res. Suppl.) **B10/11**, 423 (1985).
[24]J. S. Levinger, Phys. Lett. **82B**, 181 (1979).
[25]E. A. Whalin, Barbara Dwight Schriever, and A. O. Hanson, Phys. Rev. **101**, 377 (1956).
[26]B. Weissman and H. L. Schultz, Nucl. Phys. **A174**, 129 (1971).
[27]A. Veyssière, H. Beil, R. Bergère, P. Carlos, J. Fagot, A. Leprêtre, and A. de Miniac, Z. Phys. A **306**, 139 (1982).
[28]M. Blann, B. L. Berman, and T. T. Komoto, Phys. Rev. C **28**, 2286 (1983).